Geophysical Journal International

Geophys. J. Int. (2014) doi: 10.1093/gji/ggu098

Geophysical Journal International Advance Access published April 23, 2014

Palaeointensity determinations on rocks from Palaeoproterozoic dykes from the Kaapvaal Craton (South Africa)

V. V. Shcherbakova,[1] V. P. Shcherbakov,[1] G. V. Zhidkov[1] and N. V. Lubnina[2]

[1] *Geophysical Observatory Borok IFZ RAS, Borok, Yaroslavl, 152742, Russia. E-mail: shcherb@borok.yar.ru*

[2] *Geological Department, Lomonosov State University, Moscow, 119991, Russia*

Accepted 2014 March 14. Received 2014 March 13; in original form 2013 November 10

SUMMARY

Palaeointensity study of the Proterozoic–Archean volcanic rocks from the Kaapvaal Craton South Africa) are reported. Palaeomagnetic study of this collection was performed earlier by Olsson *et al.* Electron microscope observations, thermomagnetic and hysteresis measurements indicate the presence of single-domain and pseudo-single-domain (SD-PSD) magnetite grains as the main magnetic mineral. The samples demonstrated a very good stability to heating, the electron micrograph observations revealed magnetite–ilmenite exsolution structure. Palaeointensity determinations were obtained by Coe-modified Thellier procedure. A total 58 samples from 14 sites were studied but only seven samples from one site NL28 of the Early Proterozoic age of 1.9 Ga passed palaeointensity selection criteria. Reliable palaeointensity determinations were obtained by both Thellier and Wilson methods on 18 cubes (subsamples) from site NL28 yielding rather low mean virtual dipole moment (VDM) $= (2.82 \pm 0.12) \times 10^{22}$ Am^2 which is in agreement with the suggestion of existence of the 'Proterozoic dipole low period'.

Key words: Dynamo: theories and simulations; Magnetic mineralogy and petrology; Palaeointensity; Rock and mineral magnetism.

1 INTRODUCTION

The age of the Earth's inner core is being debated since the publication by Jacobs (1953). Yukutake (2000) and Labrosse *et al.* (2001) suggested, on the basis of Earth cooling models, that the onset of solid core formation occurred less than 2.5 Ga ago, and most likely the age of the inner core is 1 ± 0.5 Ga. Altogether with it, Labrosse *et al.* (2001) admitted that this age could be extended to 3 Ga if radioactive decay in the core is powerful enough. As was suggested by Stevenson *et al.* (1983), Hale (1987), Buffett *et al.* (1992) and Glatzmaier & Roberts (1997), the formation of the solid core should be accompanied by a notable increase in the intensity of the geomagnetic dipole moment due to the onset of chemical convection in the core. One of the methods potentially capable to detect the nucleation of the solid core is the observation of long-term variations in the palaeointensity in the deep geological past.

However, recent studies predict a considerably less pronounced increase of the dipole strength (Labrosse 2003; Aubert *et al.* 2009). Turning to empirical observations, palaeointensity data compilations for the Proterozoic and Archean also do not show a definite sign marking the onset of the inner core nucleation (Yu & Dunlop 2002; Macouin *et al.* 2003; Shcherbakova *et al.* 2008). Indeed, if for the Late and Middle Archean high virtual dipole moments (VDMs) are reported (Yoshihara & Hamano 2000; Smirnov *et al.* 2003; Tarduno *et al.* 2007), the Proterozoic field is again characterized rather low palaeointensities being in average only half of those reported for the Archean eon.

The uncertainties in both theory and empirical data impede the building of a convincing scenario for behaviour of Proterozoic and Archean geomagnetic field. The main cause for this failure is a great shortage of Precambrian palaeointensity data as can be inferred from analysis of World palaeointensity databases (http://wwwbrk.adm.yar.ru/palmag/index_e.html and http://earth.liv.ac.uk/pint/). Reputedly, many more data are needed to make a substantial progress in this important problem and the aim of this study is to improve the present database by acquiring new palaeointensity result from Palaeoproterozoic dykes in the Kaapvaal Craton (South Africa) of 1.9 Ga age.

2 PALAEOINTENSITY AND ROCK MAGNETIC INVESTIGATIONS

Results of age determinations and palaeomagnetic study of the collection from the Bushveld Igneous Complex of the Kaapvaal Craton from 27 dolerite dykes of the Palaeoproterozoic and Archean age swarms were reported in details by Olsson *et al.* (2010) and Lubnina *et al.* (2010). The palaeomagnetic directions have been calculated by means of the thermal demagnetization. The characteristic remanent magnetizations (ChRMs) were isolated over the temperature interval 440–590 °C. Noteworthy that the intensities of the ChRMs cover 95 per cent of the total natural remanent magnetizations (NRMs). The palaeopole separated in the 2.9 Ga SE-dykes, is close to the palaeopoles, obtained by Wingate (1998) and Strik *et al.* (2007) for

Table 1. Results of the palaeointensity experiments.

Sample number	H_{lab}, μT	T_1–T_2	N	Gap	q	f	k	$\sigma(k)$	H_{anc}, μT (Thellier method)	$\langle H_{anc}{}^{*}\rangle$, μT (Wilson method)
28-1-2	20	400–560	14	0.89	36.1	0.93	1.14	0.03	22.8	22.6
28-1r	20	510–560	11	0.84	48.2	0.83	0.85	0.01	16.9	
28-2	20	500–550	5	0.72	36.2	0.94	0.75	0.01	15.0	21.6
28-2-1(jr6)	20	500–540	7	0.82	20.8	0.82	0.82	0.03	16.4	
28-2-2	20	510–560	11	0.86	43.1	0.83	1.11	0.02	22.1	
28-6	20	500–575	13	0.88	32.9	0.91	0.98	0.02	19.6	16.8
28-6r	20	500–550	9	0.82	32.8	0.89	0.90	0.02	17.9	
28-7-2	20	300–550	11	0.85	27.9	0.92	0.90	0.03	18.0	18.4
28-7r	20	510–570	12	0.85	42.2	0.88	0.88	0.02	17.6	
28-8	20	520–560	5	0.65	22.4	0.80	0.66	0.02	13.1	15.8
28-8-1(jr6)	20	500–550	9	0.83	38.2	0.82	0.63	0.01	12.6	
28-8-2	20	500–560	11	0.87	32.8	0.86	1.00	0.02	20.0	
28-8-4	20	500–555	10	0.86	36.8	0.89	0.71	0.02	14.3	
28-9	20	400–535	9	0.83	34.0	0.76	0.87	0.02	17.5	16.2
28-9-2	20	515–555	9	0.85	32.2	0.80	0.82	0.02	16.5	
28-10-2	20	550–580	7	0.72	16.0	0.92	0.95	0.04	19.0	18.0
28-10n	30	500–560	6	0.66	35.2	0.95	0.64	0.01	19.2	
28-10	20	500–560	4	0.42	71.5	0.94	1.22	0.01	24.4	
Mean H_{anc} for site									17.9 ± 3.2	18.5 ± 2.7

N is the number of successive data points in the interval (T_{f1},T_{f2}) used for the calculation of H_{anc}.

2.78 Ga volcanics. The palaeopole calculated for some NE-trending dykes of the Black Ridge swarm in the NE region is close to the 1.87 Ga pole of the Kaapvaal Craton obtained by Hanson *et al.* (2004). Location of sites and summary of palaeomagnetic data are given in the table 1 of the cited paper by Lubnina *et al.* (2010).

A part of the collection (58 samples from 14 different sites) was transferred to the Geophysical Observatory 'Borok' of the Russian Academy of Sciences for palaeointensity experiments. A detailed description of the way how the Thellier palaeointensity experiments were conducted is described by Shcherbakova *et al.* (2012). In short, rock magnetic and palaeomagnetic measurements were carried out on a few cubic sister specimens of 1 cm in edge length cut from either drilled cores or hand samples. The Curie points, T_c, and the thermal stability of magnetic minerals were estimated from thermomagnetic heating–cooling cycles to incrementally higher temperatures T_i. These measurements were made with a Curie balance in an external magnetic field $B = 450$ mT.

To estimate the magnetic hardness and mineralogy of samples, measurements of magnetic susceptibility, hysteresis loop parameters, such as coercive force B_c, remanent coercive force B_{cr}, saturation magnetization M_s and remanent saturation magnetization, M_{rs}, were performed. Then, the ratios M_{rs}/M_s and B_{cr}/B_c are plotted on a Day plot (Day *et al.* 1977) to assess the domain structure (DS) of the ferromagnetic grains in the sample. The DS was estimated also by the thermomagnetic criterion by measuring the tail of a partial thermoremanent magnetization (pTRM) surviving the thermal demagnetization of the given pTRM as proposed by Shcherbakova *et al.* (2000).

Palaeointensities were determined following the experimental protocol of Coe's modified Thellier–Thellier procedure (Coe 1967). The experiment consists of a sequence of paired heatings in air to a set of increasing temperature T_i, $i = 1, \ldots n$. The first heating–cooling step to T_i takes place in zero field, the second heating is also performed in non-magnetic space following by cooling in the laboratory field, H_{lab}, equal to 20 μT. Double heatings were carried out in at least 15 steps up to 650°, pTRM checks and susceptibility measurements were performed after every second step. For each sample, the Arai-Nagata and orthogonal plots (in sample's coordinates) were constructed from the Thellier–Coe procedure data to evaluate H_{anc} and to control the fit interval for a palaeointensity determination.

In order to improve the statistics, two to four sister cubes were used from each sample. Part of the specimens were heated in an electric furnace with a residual field <50 nT, while the remaining specimens were subjected to the Thellier–Coe procedure in a full-vector three-component vibrating sample magnetometer (3D-VSM) constructed at the Geophysical Observatory 'Borok', Russia. The sensitivity of the 3D-VSM is 10^{-8} Am^2 and the maximum available external field is 0.2 mT. The rest specimens were heated in the electric furnace and measured with the JR6 magnetometer (they are marked by the label 'jr6' in Table 1). There is usually a good agreement between the results of palaeointensity experiments obtained for the sister cubes, but from different devices (Section 'Discussion and Conclusion', Table 1).

In addition to the Thellier experiments, Wilson's method (Wilson 1961) of palaeointensity determinations was also applied. Following this procedure, thermal demagnetization curves NRM(T, H_{anc}) and thermoremanent magnetization TRM(T, H_{lab}) are compared to find the temperature interval, (T_{w1}, T_{w2}), ($T_{w1} < T_{w2}$), where the graph NRM(T) is similar to the graph TRM(T). To perform the comparison, we introduced a fitting function TRM*(T) with a help of a multiplying coefficient k_w defining TRM*(T) = $k_w \times$ TRM(T). If such the interval (T_{w1}, T_{w2}) is found, $H_{anc}{}^*$ can be obtained from the coefficient of similarity, k_w = NRM(T)/TRM(T) = $H_{anc}{}^*/H_{lab}$, $T \in (T_{w1}, T_{w2})$. Noteworthy that the similarity of NRM(T) and TRM(T) curves provides a strong argument in favour of thermoremanent nature of the NRM. Examples of thermal demagnetization curves are shown in Fig. 1 (column a2–d2).

Regretfully, reliable palaeointensity determinations were obtained from only one site NL28 of 14 sites studied here. The age of NL28 rocks is 1.9 Ga as follow to Olsson *et al.* (2010): 'One U–Pb baddeleyite age from NL28 gives an age of 1865 Ma (Olsson, unpublished results), close to the general 1.90 Ga age attached to the Black Hills dyke swarm (Olsson in Soderlund *et al.* 2010). As the age of the dyke at site NL28 according to Olsson in Soderlund *et al.* (2010) is 1.90 Ga, and as the primary origin of magnetization

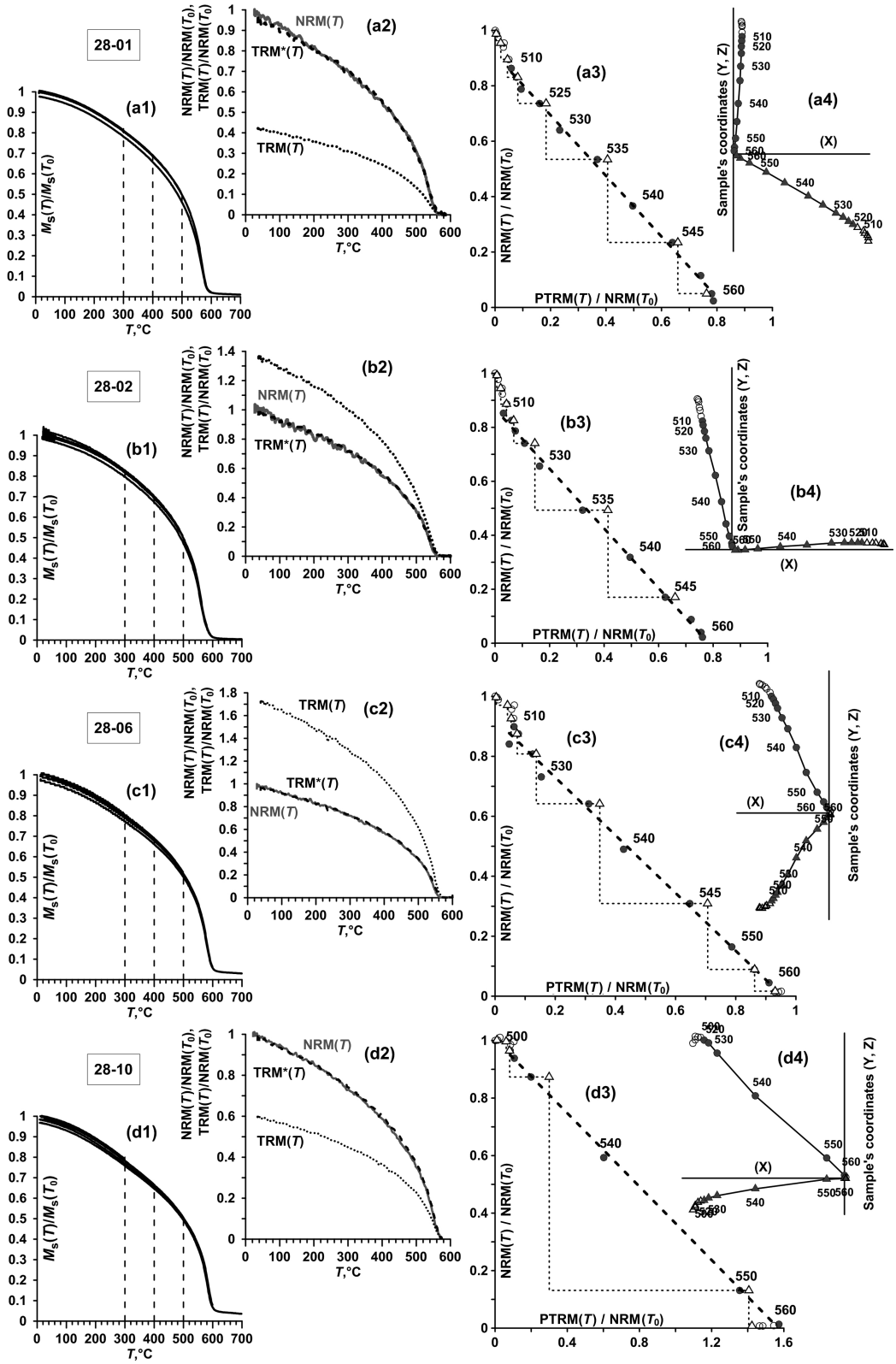

Figure 1. (a1–d1) Thermomagnetic curves $M_{si}(T)$ where vertical lines indicate the maximum temperatures T_i for each temperature loop; (a2–d2) Wilson technique. Continuous thermodemagnetization curves of NRM (full lines) and TRM acquired in $H_{lab} = 20$ μT (dot lines). Dashed line corresponds to the curve TRM* $= k_w \cdot$TRM; (a3–d3) Representative examples of accepted palaeointensity results (Arai-Nagata plots); (a4–d4) Corresponding orthogonal plots in a sample's coordinates. Numbers of samples used in the diagrams are shown in (a1–d1).

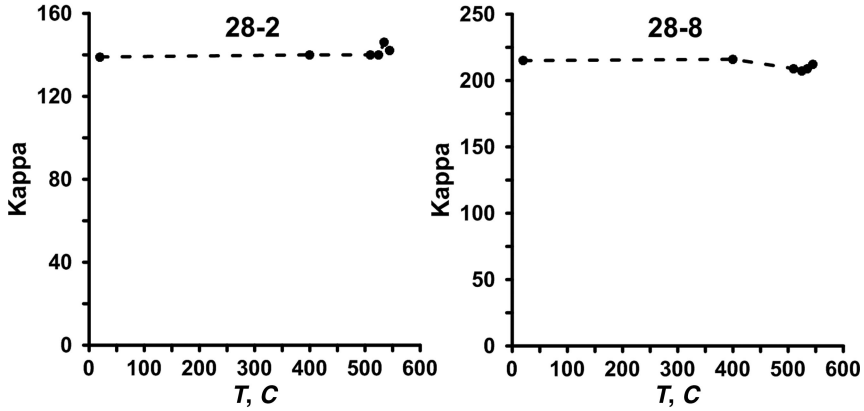

Figure 2. Samples 28-2 and 28-8. Susceptibility values measured after each second step during the Thellier procedure.

in these dykes are supported by positive contact-, conglomerate- (site NL12) and reversal tests, we conclude that the age of magnetization is 1.90 Ga.' For this reason, we will consider in details below the results obtained exclusively from this site. In all, we experimented with seven drilled cores from this site.

All samples demonstrate very similar magnetic properties and excellent stability to heating. To illustrate it, examples of the curves $M_s(T_i)$ representing heating–cooling cycles to incrementally higher temperatures T_i are shown in Fig. 1 (column a1–d1). As is seen from these curves, the samples are very stable to thermal treatment and the Curie temperatures T_c of the samples indicate magnetite as the only magnetic mineral presenting in the rocks. Indeed, from the thermomagnetic curves $M_s(T)$ (Figs 1a1–d1) and continuous thermodemagnetization curves of NRM and TRM (Figs 1a2–d2) it is seen that the Curie temperatures of the samples (determined by the maximum of the first derivative $M_s(T)$ as recommended by Fabian *et al.* 2013) are around 560–570 °C. Note that the NRM(T) curves decay almost there as well, at 560 °C.

A bit less stable to thermal treatment is the susceptibility which starts to vary after heating up to 500 °C or higher. However, the rate of these changes does not exceed 10 per cent (Fig. 2).

The values of the ratios $M_{rs}/M_s = 0.15$–0.21 and $B_{cr}/B_c = 1.7$–1.83 (Fig. 3) are confined in rather narrow intervals suggesting a good uniformity of the magnetic grains and the prevalence of fine pseudo-single (PSD) magnetic grains.

The domination of SD-PSD grains as the carriers of NRM is confirmed also by the results of application of the thermomagnetic criteria. Fig. 4 displays thermomagnetic curves of three different pTRMs imparted to the sample 28-01. As is exemplified in this figure, the pTRM(560–500) °C always has a small tail less than 5 per cent indicating the predominance of SD–fine PSD grains with blocking temperatures $T_b > 500$ °C. The two other pTRMs imparted at temperatures less than 500 °C are by an order of value weaker than the high temperature pTRM(560–500) °C and have considerable tails by the intensity up to 20 per cent of the total pTRM favouring PSD and MD DS of the grains carrying these pTRMs. Hence, the pTRM(560–500) °C constitutes the bulk of the total NRM and this observation is in full accordance with the Arai-Nagata plots (Fig. 1, column a3–d3) from which we see that NRM of all samples remains stable to the thermodemagnetization until the heating temperature increases to about 500 °C. In addition to this, note that the high values of the parameter $f > 0.8$ in the Table 1 also give a stronger line of support for a lack of MD bias (Biggin & Thomas 2003).

The suggestion of the SD-PSD nature of magnetite grains—carriers of NRM—is supported also by direct electron microscopic

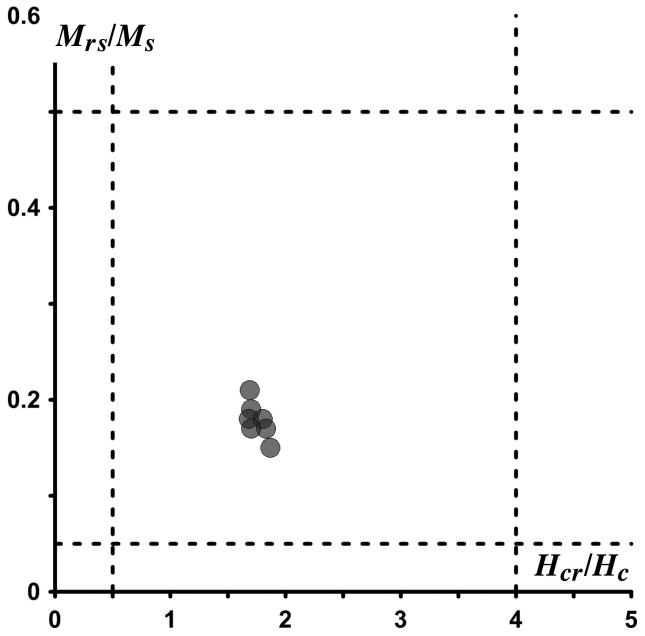

Figure 3. Day plot for the samples from the site N28.

observations. A typical example of electron micrograph taken on the sample 28-8 is shown in Fig. 5. In Fig. 5(a), we see a set of thick ilmenite lamellae (dark narrow bands) embedded in matrix which is in turn exsolved on a fine submicron scale (Fig. 5b). Besides, irregular black patterns of different sizes are present in these figures. In order to learn the composition of black patterns and the matrix, we undertook the energy dispersive spectrometry (EDS) analyses (Fig. 6). The results of the analyses are shown in the Table 2.

As is seen from the Table 2, the black patterns represent Al-rich spinel regions. Evidently, these regions are the result of exsolution of primary Al-doped titanomagnetite into Al-rich and Al-poor regions. Correspondingly, the matrix is the intergrowths of near-magnetite cells and Ti-rich lamellae. Unfortunately, an exact measurement of the Ti content in the Ti-rich phase was not possible because of the diameter of the electron beam available in our measurements, is at least 2 μm. Hence, the results of the analyses presented in Table 2 reflect the average composition over Ti-rich lamellae and Ti-poor cells.

To find the content of these two phases, the X-ray powder diffraction (XRD) was performed (Fig. 7). This diffraction pattern clearly indicates a presence of two phases: pure magnetite with a cell

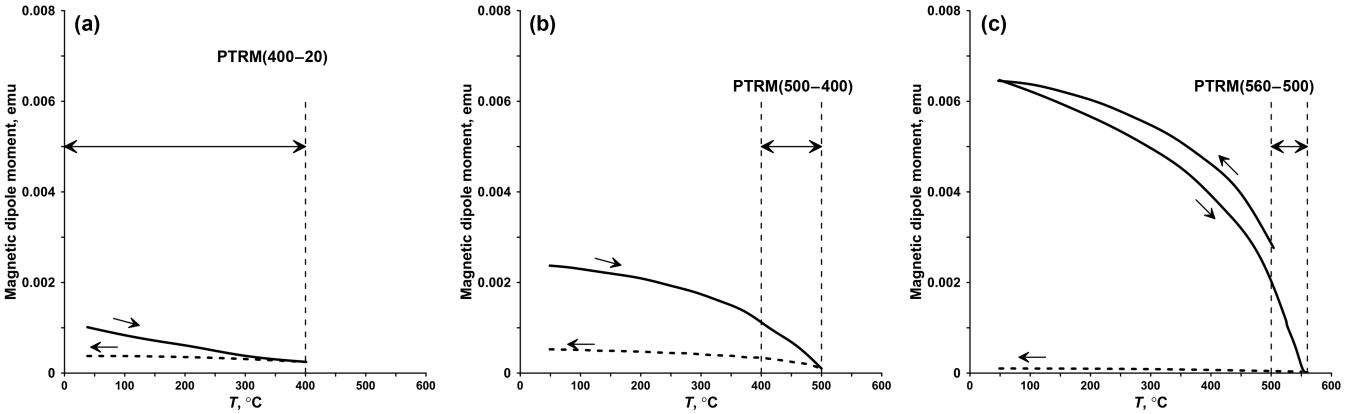

Figure 4. Application of the thermomagnetic criterion for sample 28-01. Full lines are the continuous thermodemagnetization curves of the pTRMs, dashed lines are the cooling curves of the tails of the pTRMs, both heating of pTRMs and cooling of tails of pTRMs are performed in zero field. The arrows point the direction of temperature change. The corresponding pTRMs are indicated in the diagrams.

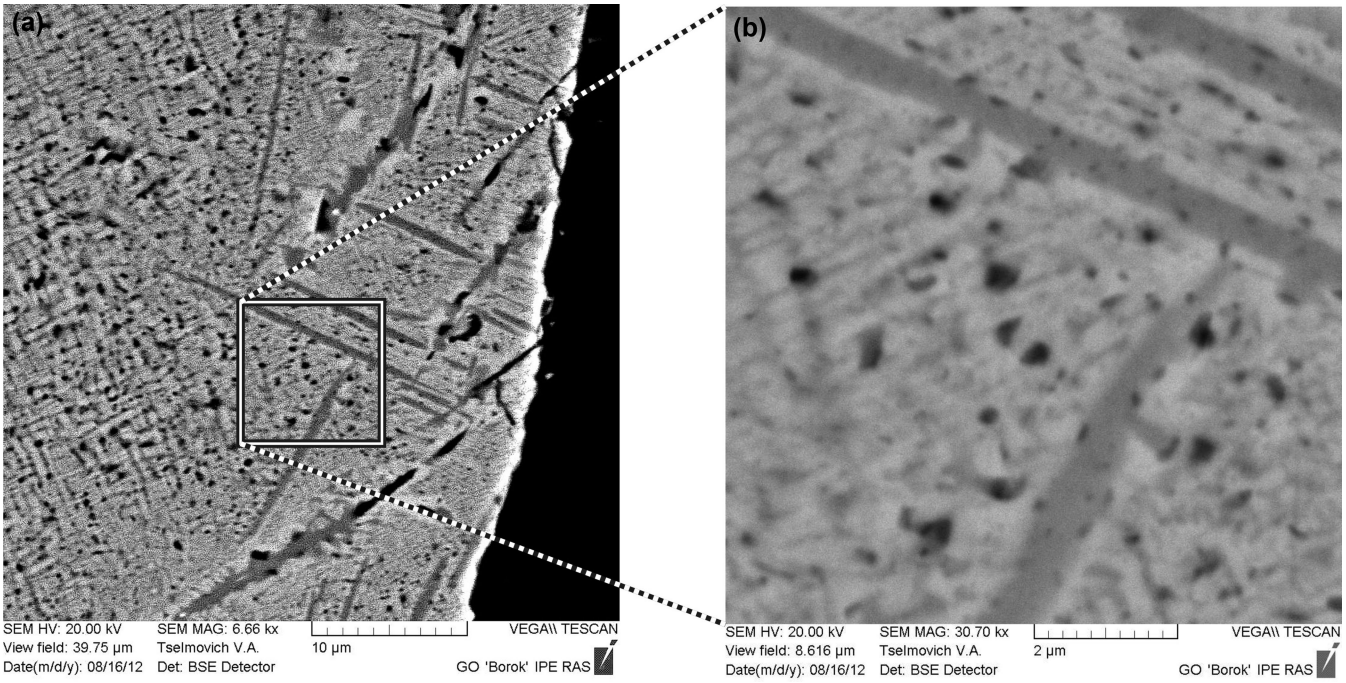

Figure 5. SEM backscattering image of a ferrimagnetic grain from the sample 28-2. (a) A general view. (b) A high magnification image of a region shown with the square in Fig. 5(a).

parameter of $a = 8.398$ Å and the rhombohedral ilmenite phase with $a = 5.0877$ Å. The lines are well shaped with no evidence of another spinel phase or significant line broadening. From here, it follows that the matrix consists of fine magnetite cells intermixed with hemoilmenite lamellae.

Noteworthy that this fine exsolution structure forms roughly rectangular array which is usually associated with the exsolution of titanomagnetite (TM) in magnetite-ulvospinel intergrowths. Hence, the plausible scenario is that the rectangular ilmenite lamellae were originally ulvospinel intergrowths, which later oxidized to ilmenite. Like this, we see the structure of the ulvospinel intergrowths, but their chemistry is now ilmenite. Another reason to state that the lamellae intergrowths are not ulvospinel is that during the subsequent heatings of samples up to 700° we see very little changes on the strong field thermomagnetic curves shown in Figs 1 (a1–d1). It means that there is no process of the homogenization of the exsolved grains which should take place in the case of the magnetite–ulvospinel intergrowths (Price 1981). (The result of the homogenization is obvious—notable decrease of T_c.)

3 RESULTS, DISCUSSION AND CONCLUSIONS

For palaeointensity determinations and analysis, the Arai-Nagata diagrams and Zijderveld orthogonal plots in sample's coordination (Zijderveld 1967) were constructed from the results of each experiment. The palaeointensity result for a sample was accepted only if it satisfied the following selection criteria:

(1) Thermomagnetic curves $M_s(T)$ show minor changes during the subsequent heatings (Figs 1a1–d1).

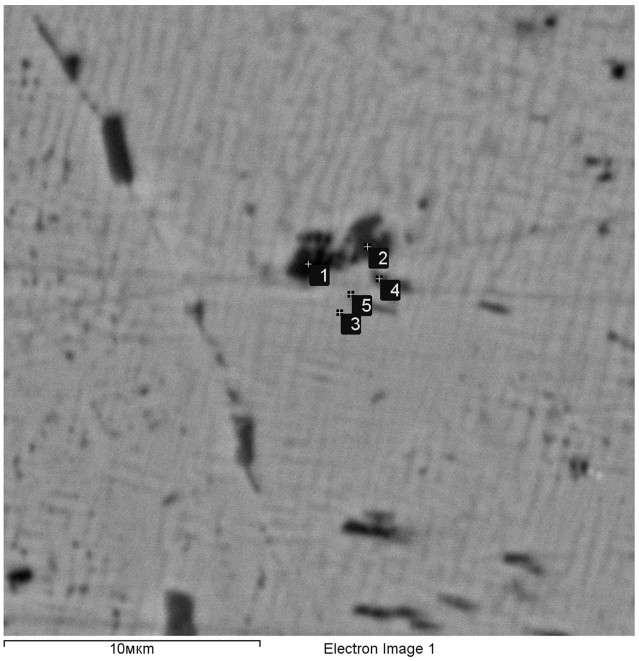

Figure 6. SEM backscattering image of a ferrimagnetic grain from the sample 28-8. The squares with numbers inside indicate the points where the EDS analyses was performed.

Table 2. Results of energy dispersive spectrometry of sample 28-8.

Point number	O	Al	Si	Ti	Fe
1	56.16	21.73	0.51	6.03	15.57
2	59.35	9.98	5.26	3.08	22.33
3	55.68	1.31	0.00	8.18	34.84
4	47.52	7.95	0.00	8.25	6.28
5	53.84	2.90	0.00	7.75	35.52

(2) There exists a wide enough temperature interval over which the curves NRM(T) and TRM(T) are similar (Figs 1a2–d2).

(3) The linear fit on the Arai-Nagata diagram over the temperature interval (T_1,T_2) used for the palaeointensity determination contains at least four consecutive data points (Figs 1a3–d3).

(4) The NRM vector is univectorial over (T_1,T_2).

(5) The fraction, f, of the NRM spanned by the linear fit is not less than 20 per cent of the total NRM.

(6) The difference between the pTRM check and the pTRM acquisition, normalized to the total NRM, must be less than 5 per cent.

(7) The susceptibility remains constant, within 10 per cent, across the temperature range, (T_1,T_2), used to determine the palaeointensity.

(8) The difference ratio (DRAT) must be less than 10 per cent.

Examples of accepted determinations are shown in Fig. 1, column (a3–d3). The dashed line in each diagram is the linear fit to the representative points of NRM versus pTRM over the temperature interval (T_1, T_2). All specimens show a sufficiently long linear segment for reliable regression analysis. The difference ratio test (Selkin & Tauxe 2000) showed that maximum DRAT for all samples in Table 1 varies between 3 and 7 per cent. It means that the pTRM checks are very close to the original pTRM's, which implies that thermochemical alteration was absent during the palaeointensity experiment.

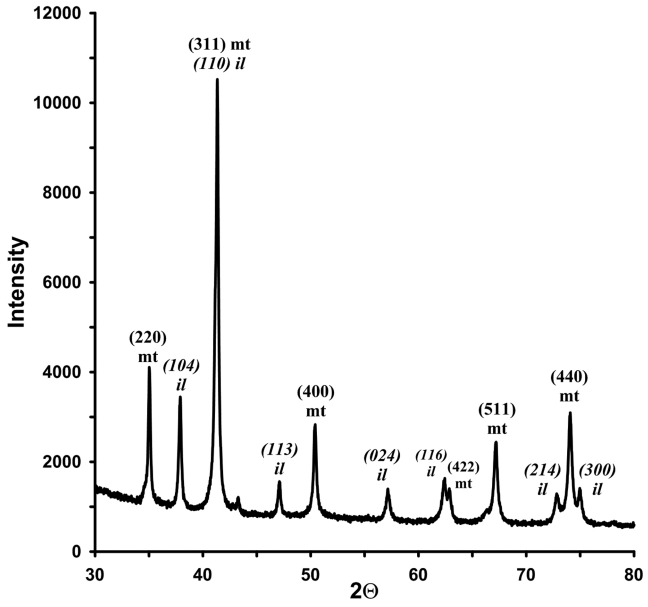

Figure 7. X-ray diffraction spectrum versus the detector angle 2θ.

The reliability of the results was also assessed by the quality factor $q = kfg/\sigma$ of Coe *et al.* (1978). Here the gap factor, g, quantifies the uniformity of the distribution of successive data points in the chosen temperature interval, in the ideal case of equidistant points, $g = (N - 2)/(N - 1)$. The coefficient $k = H_{anc}/H_{lab}$ is the absolute value of the tangent of the linear fit to the Arai-Nagata (AN) diagram over the temperature interval (T_1, T_2), the parameter σ is its standard error of k. The quality factor, $q = kfg/\sigma$, is the measure of reliability of the given palaeointensity determination. According to Coe *et al.* (1978), reliable data should have the quality factor $q \geq 5$ and we see that for the samples listed in the Table 1 q lies in the interval (16, 48) which by far exceeds this criterion.

For comparison, examples of rejected determinations are shown in Fig. 8. The samples were taken from the sites NL14, NL20 and NL22 of the age 2.65 Ga (Lubnina *et al.* 2010; Olsson *et al.* 2010). Samples from rejected sites are often characterized by significant paramagnetic contribution to the shape of strong field thermodemagnetization curves (Figs 8a1–c1). Typical Arai-Nagata diagrams of samples from these sites are displayed in Figs 8(a2–c2). The diagrams in Figs 8(a2–c2) show a very sharp decay in low-temperature range down to 300 or 500 °C depending on a sample with a very flat section at high temperatures. At the same time, the orthogonal plots are univectorial through the temperature interval (200–550) °C as is seen in Figs 8(a3–c3). So, there is no reason to choose any part of the diagrams for the palaeointensity determination. Similar diagrams with steep slope at intermediate temperatures were described by Kosterov & Prévot (1998), and recently by Shcherbakova *et al.* (2013). An explanation for this phenomenon suggests that 'the anomalous behaviour results from the reorganization of the DS of PSD grains during heating' (Kosterov & Prévot 1998). This explanation can be applied for samples 22-03 and 20-04, which are stable to the thermal treatment (Figs 8b1–c1) and show a reasonably linear Arai-Nagata plots constructed for the laboratory TRM imparted after the end of the Thellier experiment with the NRM (as exemplified in inset to Fig. 8c2). For the sample 14-01, the situation is more complex as the behaviour of the strong field thermomagnetic curves (Fig. 8a1 with the inset) points to extinction of the low-temperature phase during the heating.

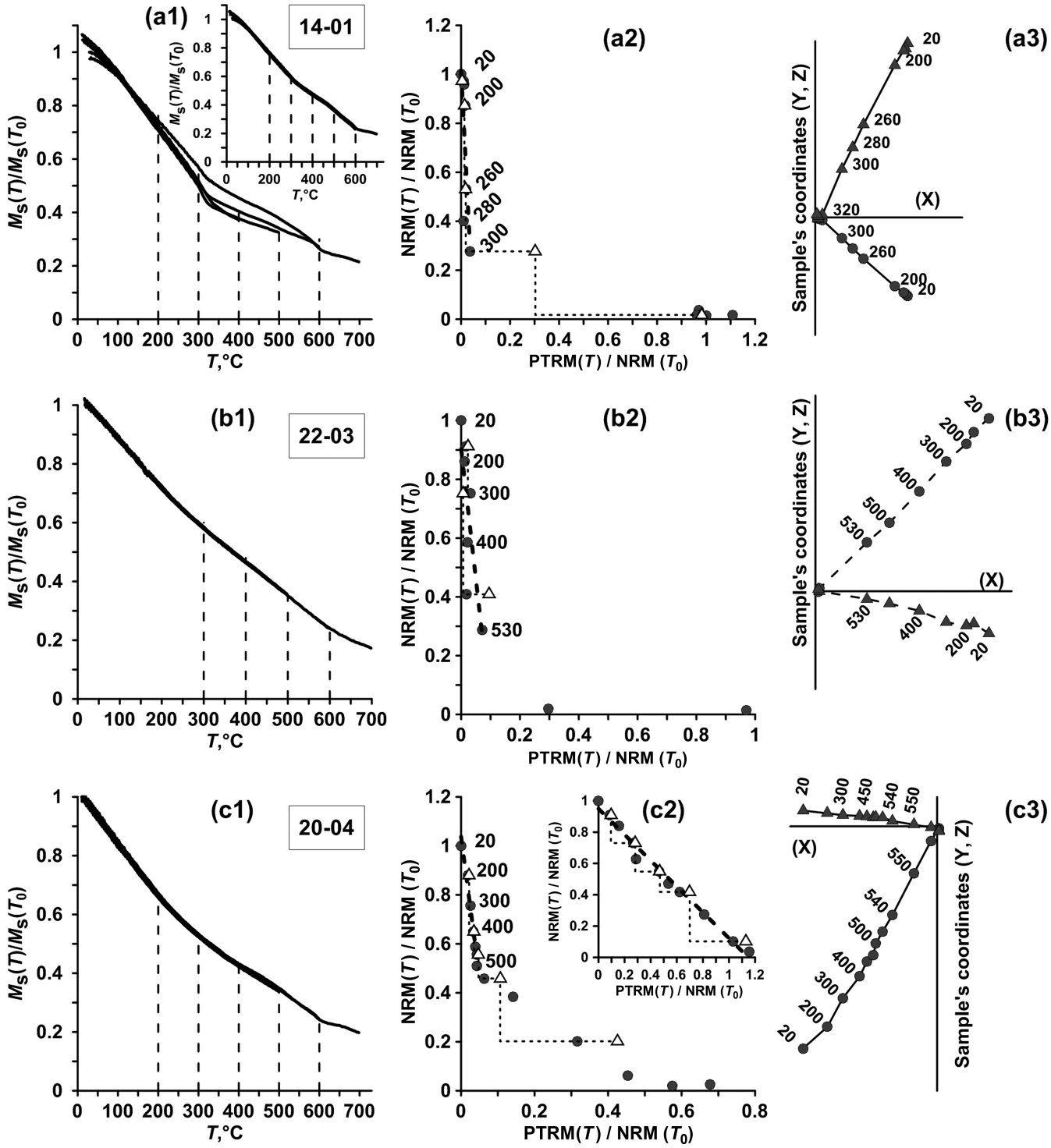

Figure 8. (a1–c1) Thermomagnetic curves $M_{si}(T)$ where vertical lines indicate the maximum temperatures T_i for each temperature loop; (a2–c2) Representative examples of rejected palaeointensity results (Arai-Nagata plots); (a3–c3) Corresponding orthogonal plots in a sample's coordinates. Numbers of samples used in the diagrams are shown in (a1–c1). Inset in (a1) shows the thermomagnetic curve $M_s(T)$ after heating to 700 °C. Inset in (c2) shows the Arai-Nagata plot for the laboratory TRM created after the Thelleier experiment with NRM was executed.

In any case, up to now there is no a reasonable physical explanation for appearance of such kind of Arai-Nagata plots with so steep slope at intermediate temperatures, besides, the physical nature of NRM leading to such diagrams, is also not clear.

A main concern in establishing the thermoremanent nature of TRM is whether the solvus temperature of titanomagnetite occurs above or below the Curie temperature of exsolved titanomagnetite grains (Smirnov & Tarduno 2005). According to Price 1981, T_s can be less than 500° but other published data give considerably higher consolute (peak solvus) temperatures. Namely, $T_s = 650°$ at TM content $(Fe_3O_4)_{35}(Fe_2TiO_4)_{65}$ (Rumble 1970); $T_s = 565°$ at TM content $(Fe_3O_4)_{55}(Fe_2TiO_4)_{45}$ (Lindsley 1981); $T_s = 600°$ at

TM content $(Fe_3O_4)_{58}(Fe_2TiO_4)_{42}$ (Kawai 1956), $T_s = 600^\circ$ at TM content $(Fe_3O_4)_{63}(Fe_2TiO_4)_{37}$ (Vincent 1957; Basta 1960).

From the cited data, one cannot draw a definite conclusion on the question whether or not the exsolution occurs above or below the Curie temperature of exsolved titanomagnetite grains, rather it looks like the exsolution can happen by both way depending on the actual situation. However, remind that the ferromagnetic grains in our study contain a notable amount of Al and other minor elements. However, Al-bearing titanomagnetites are reported to have higher T_s than that of the pure TM (Turnock & Eugster 1962; Petrochilos 2010). This observation promotes acquisition of TRM (not TCRM - thermochemical remanent magnetization) of the exsolved magnetite-rich phase in our case.

Other reasons in favour of a TRM origin for the NRM of the samples studied here are provided by the strong similarity of the NRM–TRM plots and the exceptional quality and linearity of the Arai-Nagata plots. The property of linearity is essential for the 'true' Arai-Nagata plots when the NRM is indeed of the thermoremanent origin. However, the existence of this property is under serious doubts when the TCRM is considered. To support this, remind that the only developed theoretical scheme for TCRM acquisition is the grain growth mechanism of acquisition of the TCRM (Kobayashi 1962) which predicts for non-interacting SD grains the ratio TCRM/TRM $= H_K(T_b)/H_K(T_{TCRM}) < 1$ (Stacey & Banerjee 1974), where T_{TCRM} is the temperature of the TCRM acquisition, and H_K is the coercive force of a grain. According to this relationship, Arai-Nagata plot of (TCRM versus laboratory TRM) should have downward curvature which is not at all seen in the plots (a3–d3) in Fig. 1.

Despite these arguments, one cannot completely rule out the possibility that NRMs in our collection rocks are yet TCRMs. Indeed, if TRM and TCRM have similar blocking temperature spectrum, they will be undistinguishable from the point of view of Thellier and Wilson experiments. However, if so, one has to admit that the well-known model of acquisition of TCRM by Kobayashi (1962), is wrong and for some unknown reasons TRM and TCRM have completely similar (or almost similar) blocking temperature spectrum. A comprehensive answer to this question can be received only after extensive experimental and theoretical studies of possible mechanisms of the TCRM acquisition will be done.

Reliable palaeointensity determinations were obtained by Thellier and Wilson methods on 18 sister cubes from seven samples yielding palaeofields H_{anc} lying in the interval 13–25 μT (Table 1) from the site NL28. The last line of the Table 1 presents the mean site values of H_{anc} obtained by these methods.

In accordance with the strong thermostability of NRMs of the samples sampled from the site NL28, demonstrated in the previous section, the positions of checkpoints on the Arai-Nagata diagrams are found to be very close to the initial pTRM values (Fig. 1, column a3–d3).

Two slopes can be distinguished in the Arai-Nagata diagrams in temperature intervals (T_r, 510) °C and (510, 560) °C, correspondingly (Fig. 1, a3–d3). Note that they are not equivalent in the sense of intensity of NRM: the low-temperature part is much smaller. The same two components are seen also in the orthogonal plots (Fig. 1, a4–d4). Noteworthy the low-temperature component is associated with multidomain pTRM tails behaviour as is revealed by the thermomagnetic criteria. Indeed, the two pTRMs imparted at temperatures below 500 °C are very weak in intensity and have considerable tails (Figs 4a and b) indicating the PSD and MD DS of the grains carrying of these pTRMs (Shcherbakova *et al.* 2000). A similar situation was observed by Carvallo *et al.* (2003).

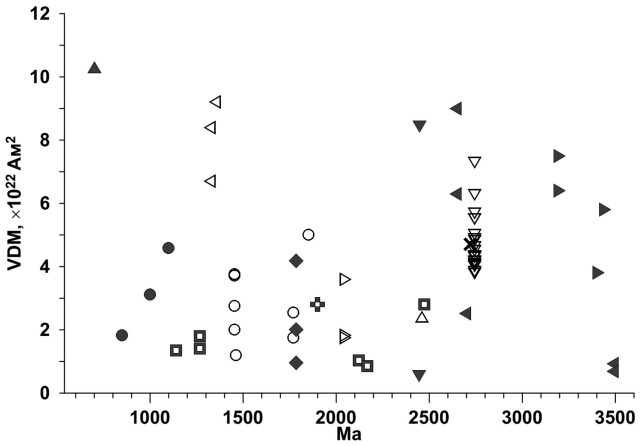

✣ – this work; ○ – Shcherbakova *et al.* (2004, 2006a, 2006b, 2008); ✕ – Biggin *et al.* (2009); ◆ – Donadini *et al.* (2011); ◘ – Macouin *et al.* (2003, 2006); △ – McArdle *et al.* (2004); ▲ – Salminen *et al.* (2006); ▽ – Selkin *et al.* (2008); ▼ – Smirnov *et al.* (2003), Smirnov & Tarduno (2005); ▷ – Sumita *et al.* (2001); ▶ – Tarduno *et al.* (2007, 2010); ◁ – Thomas (1993), Thomas & Piper (1995); ◀ – Yoshihara & Hamano (2000, 2004); ● – Yu & Dunlop (2001, 2002).

Figure 9. Summary of the Precambrian VDMs from this study and from published sources obtained by the Thellier method and selected by the criteria by Perrin & Shcherbakov (1997).

Using now the known average inclination $I = -67.6^\circ$ for the NL28 site (Lubnina *et al.* 2010) and the mean site Thellier palaeointensity $H_{ans} = 17.9$ μT (Table 1), it yields the mean VDM ± standard error of the mean $= (2.82 \pm 0.12) \times 10^{22}$ Am^2. This value is in a good agreement with the results of the Wilson's method which produced practically the same mean VDM.

Fig. 9 displays the Archaean/Proterozoic palaeointensity data presented in the World palaeointensity databases (http://wwwbrk.adm.yar.ru/palmag/index_e.html and http://earth.liv.ac.uk/pint/). The data are selected according to the criteria of reliability formulated by Perrin & Shcherbakov (1997): only Thellier-type determinations are considered; at least three samples are used for the VDM calculation; the standard error of site averaging of H_{anc} should not exceed 15 per cent (the criterion of internal consistency). At all, 59 Thellier-type palaeointensity determinations were found to pass these selection criteria for the Archaean/Proterozoic rocks. As is seen in the Fig. 9, the Achaean data display rather higher VDM values with the mean VDM $= 6 \times 10^{22}$ Am^2, comparable to those of observed in the Cenozoic. On contrary, the Proterozoic VDMs, with the exception of the data reported by Thomas (1993), Thomas & Piper (1995) and Smirnov *et al.* (2003), are considerably less than the most of the Cenozoic VDM values giving the mean VDM only 3.2×10^{22} Am^2.

The distributions of VDMs for the Late/Middle Archean and Proterozoic are presented in the histograms in Figs 10(a) and (b). As is seen, the histograms in Fig. 10 demonstrate a pronounced non-monotonic and rugged shape, which probably indicates that the data are too scarce and the statistics made after them is insufficient. Still, the mean VDMs over the Proterozoic and Late/Middle Archean, equal to $(3.2 \pm 0.45) \times 10^{22}$ Am^2 and $(6.02 \pm 0.38) \times 10^{22}$ Am^2, correspondingly, differ too much to ignore the difference as the triple sum of the standard errors exceeds the difference between the means. The observation that low field prevailed during the Proterozoic, while it was high in the Late/Middle Archean, was already emphasized by Macouin *et al.* (2004), Shcherbakova *et al.* (2008) and Biggin *et al.* (2009). Because of the average geomagnetic field strength seems to be high again in the most of the Phanerozoic,

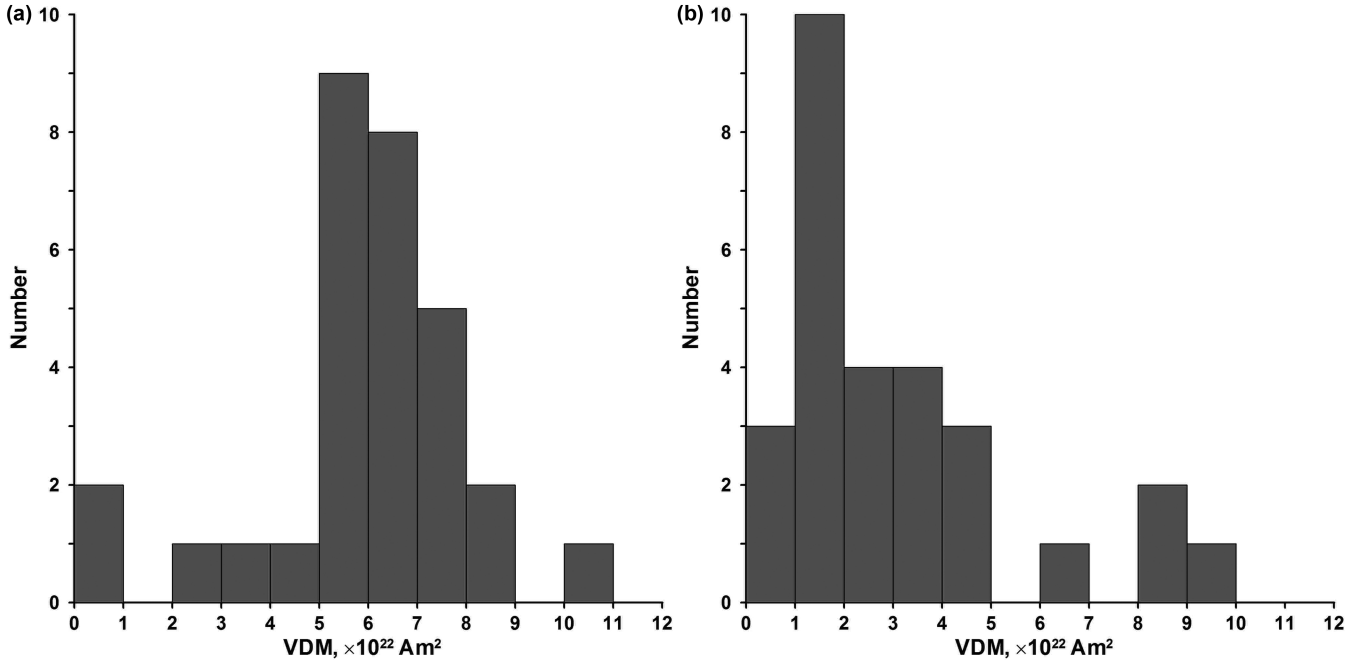

Figure 10. Histograms of VDMs. (a) Meso- and Neo- Archean data; (b) Proterozoic data.

Biggin *et al.* (2009) hypothesized the existence of a special 'Proterozoic dipole low period' in analogy with the long existing hypothesize of the 'Mesozoic dipole low' suggested by Prevot *et al.* (1990). In this line, our data provide another confirmation of low field domination in the Early Proterozoic.

In support of this idea, Biggin *et al.* (2009) proposed a related three-stage evolution in core dynamics with vigorous thermal convection in the Archean, weak thermal convection in the Proterozoic and strong compositional convection after the inner core nucleated.

A principle possibility of such the scenario when the field strength gradually decreases from the Archean through the Early Proterozoic and increases again after the inner core nucleation was demonstrated recently by Aubert *et al.* (2009), who analysed the palaeoevolution of the geodynamo by combining core thermodynamics with scaling analysis of numerical dynamo simulations. To consider the problem in very general terms, the authors introduced high and low-power scenarios for the Earth cooling evolution in the geological past. As occurred, the evolution of intensity of the dipole moment with time shows different trends for these end-members scenarios (see fig. 11b from Aubert *et al.* 2009). For the high-power case, the field intensity increases slowly from the onset of dynamo action till the present time. The nucleation of the inner core in this case starts rather late, at ≈0.8 Ga but this event has little effect on the geomagnetic field intensity. Probability of this kind of scenario was recently supported by Pozzo *et al.* (2012). For the low-power scenario, the model predicts the decrease of the dipole moment until the Middle Proterozoic where the inner core nucleates at about 1.8 Ga and the field starts to increase for a while. However, later, in the Middle Proterozoic, the field intensity returns to the decreasing trend again.

Certainly, the real cooling process can considerably differ from these scenarios being a combination of them. Nevertheless, from the available Precambrian palaeointensity records, where the relatively high Archean field gives way to the low Proterozoic field, the preference should be given rather to the low-power scenario, at least, on the early stage of the geological history. Regretfully, both end-member cooling scenarios predict a relatively weak increase in the palaeointensity as a result of the Earth's inner core growth (Aubert *et al.* 2009). If so, it leaves little hope to detect a possible signature associated with the onset of the inner core crystallization from the available scarce and scattering palaeomagnetic data until new numerous reliable determinations of the Precambrian field will be obtained.

ACKNOWLEDGEMENTS

The authors are grateful to Pierre Camps and an anonymous referee for the valuable comments made to this paper, Suzanne McEnroe for the fruitful discussion and V. Tselmovich for the help in producing the electronic micrographs. This study was supported by Ministry of Science and Education of the Russian federation, contract # 14.Z50.31.0017.

REFERENCES

Aubert, J., Labrosse, S. & Poitou, C., 2009. Modelling the palaeo-evolution of the geodynamo, *Geophys. J. Int.,* **179**(3), 1414–1428.

Basta, E.Z., 1960. Natural and synthetic titanomagnetites (the system Fe_3O_4–Fe_2TiO_4–$FeTiO_3$), *N. Jb. Miner*. **94,** 1017–1048.

Biggin, A.J. & Thomas, D.N., 2003. The application of acceptance criteria to results of Thellier palaeointensity experiments performed on samples with pseudo-single-domain-like characteristics, *Phys. Earth planet. Inter.,* **138**(3–4), 279–287.

Biggin, A.J., Strik, G. & Langereis, C.G., 2009. The intensity of the geomagnetic field in the late-Archaean: new measurements and an analysis of the updated IAGA palaeointensity database, *Earth Planets Space,* **61**(1), 9–22.

Buffett, B.A., Huppert, H.E., Lister, J.R. & Woods, A.W., 1992. Analytical model for solidification of the Earth's core, *Nature,* **356**(6367), 329–331.

Carvallo, C., Camps, P., Ruffet, G., Henry, B. & Poidras, T., 2003. Mono Lake or Laschamp geomagnetic event recorded from lava flows in Amsterdam Island (southeastern Indian Ocean), *Geophys. J. Int.,* **154**(3), 767–782.

Coe, R.S., 1967. The determination of paleointensities of the Earth's magnetic field with special emphasize on mechanisms which could cause nonideal behavior in Thellier's method, *J. Geomag. Geoelectr.,* **19**(3), 157–178.

Coe, R.S., Grommé, S. & Mankinen, E.A., 1978. Geomagnetic paleointensities from radiocarbon-dated lava flows on Hawaii and the question of the Pacific nondipole low, *J. geophys. Res.,* **83**(B4), 1740–1756.

Day, R., Fuller, M. & Schmidt, V.A., 1977. Hysteresis properties of titanomagnetites: grain-size and compositional dependence, *Phys. Earth planet. Inter.,* **13**(4), 260–267.

Donadini, F., Elming, S.-Å., Tauxe, L. & Hålenius, U., 2011. Paleointensity determination on a 1.786 Ga old gabbro from Hoting, Central Sweden, *Earth planet. Sci. Lett.,* **309**(3–4), 234–248.

Fabian, K., Shcherbakov, V.P. & McEnroe, S.A., 2013. Measuring the Curie temperature, *Geochem. Geophys. Geosyst.,* **14**(4), 947–961.

Glatzmaier, G.A. & Roberts, P.H., 1997. Simulating the geodynamo, *Contemp. Phys.,* **38**(4), 269–288.

Hale, C.J., 1987. Palaeomagnetic data suggest link between the Archaean-Proterozoic boundary and inner-core nucleation, *Nature,* **329**(6136), 233–237.

Hanson, R.E. *et al.*, 2004. Paleoproterozoic intraplate magmatism and basin development on the Kaapvaal Craton: age, paleomagnetism and geochemistry of ∼1.93 to ∼1.87 Ga post-Waterberg dolerites, *South Afr. J. Geol.,* **107**(1–2), 233–254.

Jacobs, J.A., 1953. The Earth's inner core, *Nature,* **172**(4372), 297–298.

Kawai, N., 1956. Subsolidus phase relation in titanomagnetite and its significance in rock-magnetism, in *Proceedings of the 20th International Geological Congress*, Tokyo, Section 11A, pp. 103–120.

Kobayashi, K., 1962. Crystallization or chemical remanent magnetization, in *Proceedings of the Benedum Earth Magnetism Symposium*, University of Pittsburg, pp. 107–112.

Kosterov, A.A. & Prévot, M., 1998. Possible mechanisms causing failure of Thellier palaeointensity experiments in some basalts, *Geophys. J. Int.,* **134**(2), 554–572.

Labrosse, S., 2003. Thermal and magnetic evolution of the Earth's core, *Phys. Earth planet. Inter.,* **140**(1–3), 127–143.

Labrosse, S., Poirier, J.-P. & Le Mouël, J.-L., 2001. The age of the inner core, *Earth planet. Sci. Lett.,* **190**(3–4), 111–123.

Lindsley, D.H., 1981. Some experiments pertaining to the magnetite-ulvospinel miscibility gap, *Am. Mineral.*, **66,** 759–762.

Lubnina, N., Richard, E., Martin, K. & Ulf, S., 2010. Paleomagnetic study of NeoArchean–Paleoproterozoic dykes in the Kaapvaal Craton, *Precambrian Res.,* **183,** 523–552.

Macouin, M., Valet, J.P., Besse, J., Buchan, K., Ernst, R., LeGoff, M. & Scharer, U., 2003. Low paleointensities recorded in 1 to 2.4 Ga Proterozoic dykes, Superior Province, Canada, *Earth planet. Sci. Lett.,* **213**(1–2), 79–95.

Macouin, M., Valet, J.-P. & Besse, J., 2004. Long-term evolution of the geomagnetic dipole moment, *Phys. Earth planet. Inter.,* **147**(2–3), 239–246.

Macouin, M., Valet, J.P., Besse, J. & Ernst, R.E., 2006. Absolute paleointensity at 1.27 Ga from the Mackenzie dyke swarm (Canada), *Geochem. Geophys. Geosyst.,* **7**(1), Q01H21, doi:10.1029/2005gc000960.

McArdle, N.J., Halls, H.C. & Shaw, J., 2004. Rock magnetic studies and a comparison between microwave and Thellier palaeointensities for Canadian Precambrian dykes, *Phys. Earth planet. Inter.,* **147**(2–3), 247–254.

Olsson, J.R., Söderlund, U., Klausen, M.B. & Ernst, R.E., 2010. U–Pb baddeleyite ages linking major Archean dyke swarms to volcanic-rift forming events in the Kaapvaal craton (South Africa), and a precise age for the Bushveld Complex, *Precambrian Res.,* **183,** 490–500.

Perrin, M. & Shcherbakov, V.P., 1997. Paleointensity of the Earth's magnetic field for the past 400 Ma: evidence for a dipole structure during the Mesozoic low, *J. Geomag. Geoelectr.,* **49**(4), 601–614.

Petrochilos, L.T., 2010. Experimental and analytical studies of titanomagnetite in synthetic and natural samples, *A thesis submitted to the graduate division of the University of Hawaii in partial fulfillment of the requirements for the degree of master of science in geology and geophysics,* The University of Hawaii.

Pozzo, M., Davies, C., Gubbins, D. & Alfe, D., 2012. Thermal and electrical conductivity of iron at Earth's core conditions, *Nature,* **485**(7398), 355–358.

Prevot, M., Derder, M.E.-M., McWilliams, M. & Thompson, J., 1990. Intensity of the Earth's magnetic field: evidence for a Mesozoic dipole low, *Earth planet. Sci. Lett.,* **97**(1–2), 129–139.

Price, G.D., 1981. Subsolidus phase relations in the titanomagnetite solid solution series, *Am. Mineral.,* **66,** 751–758.

Rumble, D., 1970. Thermodynamic analysis of phase equilibria in the system Fe_2TiO_4–Fe_3O_4–TiO_2, *Year Book – Carnegie Inst. Wash.,* **69,** 198–207.

Salminen, J., Donadini, F., Pesonen, L.J., Masaitis, V.L. & Naumov, M.V., 2006. Paleomagnetism and petrophysics of the Jänisjärvi impact structure, Russian Karelia, *Meteorit. Planet. Sci.,* **41**(12), 1853–1870.

Scherbakova, V.V., Zhidkov, G.V., Latyshev, A.V. & Scherbakov, V.P., 2013. Estimating the variations in paleointensity from the Siberian traps of Maymecha-Kotui and Norilsk regions, *Izv. Phys. Solid Earth,* **49**(4), 488–504.

Selkin, P.A. & Tauxe, L., 2000. Long-Term variations in palaeointensity, *Phil. Trans. R. Soc. Lond., A.,* **358,** 1065–1088.

Selkin, P.A., Gee, J.S., Meurer, W.P. & Hemming, S.R., 2008. Paleointensity record from the 2.7 Ga Stillwater Complex, Montana, *Geochem. Geophys. Geosyst.,* **9**(12), Q12023, doi:10.1029/2008gc001950.

Shcherbakova, V.V., Shcherbakov, V.P. & Heider, F., 2000. Properties of partial thermoremanent magnetization in pseudosingle domain and multidomain magnetite grains, *J. geophys. Res.,* **105**(B1), 767–781.

Shcherbakova, V.V., Zhidkov, G.A., Pavlov, V.E. & Zemtsov, V.A. 2004. The paleointensity determinations on Early Proterozoic rocks of South Karelia, In *Palaeomagnetism and Rock Magnetism: The Theory, Practice, Experiment,* pp. 61–66, Kazan State University [in Russian].

Shcherbakova, V.V., Pavlov, V.E., Shcherbakov, V.P., Neronov, I. & Zemtsov, V.A., 2006a. Paleomagnetic studies and estimation of geomagnetic paleointensity at the early/middle Riphean boundary in rocks of the Salmi Formation (North Ladoga area), *Izv. Phys. Solid Earth,* **42**(3), 233–243.

Shcherbakova, V.V., Shcherbakov, V.P., Didenko, A.N. & Vinogradov, Y.K., 2006b. Determination of the paleointensity in the Early Proterozoic from granitoids of the Shumikhinskii complex of the Siberian craton, *Izv. Phys. Solid Earth,* **42**(6), 521–529.

Shcherbakova, V.V., Lubnina, N.V., Shcherbakov, V.P., Mertanen, S., Zhidkov, G.V., Vasilieva, T.I. & Tselmovich, V.A., 2008. Palaeointensity and palaeodirectional studies of early Riphaean dyke complexes in the Lake Ladoga region (Northwestern Russia), *Geophys. J. Int.,* **175**(2), 433–448.

Shcherbakova, V.V., Bakhmutov, V.G., Shcherbakov, V.P., Zhidkov, G.V. & Shpyra, V.V., 2012. Palaeointensity and palaeomagnetic study of Cretaceous and Palaeocene rocks from Western Antarctica, *Geophys. J. Int.,* **189**(1), 204–228.

Smirnov, A.V. & Tarduno, J.A., 2005. Thermochemical remanent magnetization in Precambrian rocks: are we sure the geomagnetic field was weak? *J. geophys. Res.,* **110**(B6), B06103, doi:10.1029/2004jb003445.

Smirnov, A.V., Tarduno, J.A. & Pisakin, B.N., 2003. Paleointensity of the early geodynamo (2.45 Ga) as recorded in Karelia: a single-crystal approach, *Geology,* **31**(5), 415–418.

Soderlund, U., Hofmann, A., Klausen, M.B., Olsson, J.R. & Ernst, R.E., 2010. Towards a complete magmatic barcode for the Zimbabwe craton: baddeleyite U–Pb dating of regional dolerite dike swarms and sill provinces, *Precambrian Res.,* **183,** 388–398.

Stacey, F.D. & Banerjee, S.K., 1974. *The Physical Principles of Rock Magnetism,* Elsevier, 195 pp.

Stevenson, D.J., Spohn, T. & Schubert, G., 1983. Magnetism and thermal evolution of the terrestrial planets, *Icarus,* **54**(3), 466–489.

Strik, G., de Wit, M.J. & Langereis, C.G., 2007. Palaeomagnetism of the Neoarchaean Pongola and Ventersdorp Supergroups and an appraisal of the 3.0–1.9 Ga apparent polar wander path of the Kaapvaal Craton, Southern Africa, *Precambrian Res.,* **153**(1–2), 96–115.

Sumita, I., Hatakeyama, T., Yoshihara, A. & Hamano, Y., 2001. Paleomagnetism of late Archean rocks of Hamersley basin, Western Australia and the paleointensity at early Proterozoic, *Phys. Earth planet. Inter.,* **128**(1–4), 223–241.

Tarduno, J.A., Cottrell, R.D., Watkeys, M.K. & Bauch, D., 2007. Geomagnetic field strength 3.2 billion years ago recorded by single silicate crystals, *Nature,* **446**(7136), 657–660.

Tarduno, J.A. *et al.*, 2010. Geodynamo, solar wind, and magnetopause 3.4 to 3.45 billion years ago, *Science,* **327**(5970), 1238–1240.

Thomas, D.N. & Piper, J.D.A., 1995. Evidence for the existence of a transitional geomagnetic field recorded in a Proterozoic lava succession, *Geophys. J. Int.,* **122**(1), 266–282.

Thomas, N., 1993. An integrated rock magnetic approach to the selection or rejection of ancient basalt samples for palaeointensity experiments, *Phys. Earth planet. Inter.,* **75**(4), 329–342.

Turnock, A.C. & Eugster, H.P., 1962. Fe-Al oxides: phase relations below 1000°C, *J. Petrol.,* **3,** 533–565.

Vincent, E.A., Wright, J.B., Chevallier, R. & Mathieu, S., 1957. Heating experiments on some natural titanoferous magnetites, *Mineral. Mag.,* **31**(239), 624–655.

Wilson, R.L., 1961. The thermal demagnetization of natural magnetic moments in rocks, *Geophys. J. R. astr. Soc.,* **5**(1), 45–58.

Wingate, M.T.D., 1998. A palaeomagnetic test of the Kaapvaal-Pilbara (Vaalbara) connection at 2.78 Ga, *S. Afr. J. Geol.,* **101**(4), 257–274.

Yoshihara, A. & Hamano, Y., 2000. Intensity of the Earth's magnetic field in late Archean obtained from diabase dikes of the Slave Province, Canada, *Phys. Earth planet. Inter.,* **117**(1–4), 295–307.

Yoshihara, A. & Hamano, Y., 2004. Paleomagnetic constraints on the Archean geomagnetic field intensity obtained from komatiites of the Barberton and Belingwe greenstone belts, South Africa and Zimbabwe, *Precambrian Res.,* **131**(1–2), 111–142.

Yu, Y. & Dunlop, D.J., 2001. Paleointensity determination on the Late Precambrian Tudor Gabbro, Ontario, *J. geophys. Res.,* **106**(B11), 26 331–26 343.

Yu, Y. & Dunlop, D.J., 2002. Multivectorial paleointensity determination from the Cordova Gabbro, southern Ontario, *Earth planet. Sci. Lett.,* **203**(3–4), 983–998.

Yukutake, T., 2000. The inner core and the surface heat flow as clues to estimating the initial temperature of the Earth's core, *Phys. Earth planet. Inter.,* **121**(1–2), 103–137.

Zijderveld, J.D.A., 1967. The natural remanent magnetizations of the exeter volcanic traps (Permian, Europe), *Tectonophysics,* **4**(2), 121–153.